

Multi-function terahertz wave manipulation utilizing Fourier convolution operation metasurface

Min Zhong(仲敏) and Jiu-Sheng Li(李九生)

Citation: Chin. Phys. B, 2022, 31 (**5**): 054207. DOI: 10.1088/1674-1056/ac46c0
Journal homepage: http://cpb.iphy.ac.cn; http://iopscience.iop.org/cpb

What follows is a list of articles you may be interested in

Creation of multi-frequency terahertz waves by optimized cascaded difference frequency generation

Zhong-Yang Li(李忠洋), Jia Zhao(赵佳), Sheng Yuan(袁胜), Bin-Zhe Jiao(焦彬哲), Pi-Bin Bing(邴丕彬), Hong-Tao Zhang(张红涛), Zhi-Liang Chen(陈治良), Lian Tan(谭联), and Jian-Quan Yao(姚建铨)
Chin. Phys. B, 2022, 31 (**4**): 044205. DOI: 10.1088/1674-1056/ac29b4

High-sensitive terahertz detection by parametric up-conversion using nanosecond pulsed laser

Yuye Wang(王与烨), Gang Nie(聂港), Changhao Hu(胡常灏), Kai Chen(陈锴), Chao Yan(闫超), Bin Wu(吴斌), Junfeng Zhu(朱军峰), Degang Xu(徐德刚), and Jianquan Yao(姚建铨)
Chin. Phys. B, 2022, 31 (**2**): 024204. DOI: 10.1088/1674-1056/ac2d20

Efficient manipulation of terahertz waves by multi-bit coding metasurfaces and further applications of such metasurfaces

Yunping Qi(祁云平) Baohe Zhang(张宝和), Jinghui Ding(丁京徽), Ting Zhang(张婷), Xiangxian Wang(王向贤), and Zao Yi(易早)
Chin. Phys. B, 2021, 30 (**2**): 024211. DOI: 10.1088/1674-1056/abd6fc

Multi-functional vanadium dioxide integrated metamaterial for terahertz wave manipulation

Jian-Xing Zhao(赵建行), Jian-Lin Song(宋建林), Yao Zhou(周姚), Rui-Long Zhao(赵瑞龙), Yi-Chao Liu(刘艺超), Jian-Hong Zhou(周见红)
Chin. Phys. B, 2020, 29 (**9**): 094205. DOI: 10.1088/1674-1056/abab6f

Active metasurfaces for manipulatable terahertz technology

Jing-Yuan Wu(吴静远), Xiao-Feng Xu(徐晓峰), Lian-Fu Wei(韦联福)
Chin. Phys. B, 2020, 29 (**9**): 094202. DOI: 10.1088/1674-1056/aba613

Multi-function terahertz wave manipulation utilizing Fourier convolution operation metasurface

Min Zhong(仲敏) and Jiu-Sheng Li(李九生)†

Center for THz Research, China Jiliang University, Hangzhou 310018, *China*

(Received 25 October 2021; revised manuscript received 11 December 2021; accepted manuscript online 29 December 2021)

We propose a novel metasurface based on a combined pattern of outer C-shaped ring and inner rectangular ring. By Fourier convolution operation to generating different predesigned sequences of metasurfaces, we realize various functionalities to flexible manipulate terahertz waves including vortex terahertz beam splitting, anomalous vortex terahertz wave deflection, vortex terahertz wave splitting and deflection simultaneously. The incident terahertz wave can be flexibly controlled in a single metasurface. The designed metasurface has an extensive application prospect in the field of future terahertz communication and sensing.

Keywords: Fourier convolution operation metasurface, terahertz wave, flexible manipulation

PACS: 42.50.Tx, 03.65.Vf, 07.05.Tp **DOI:** 10.1088/1674-1056/ac46c0

1. Introduction

In recent years, metasurfaces have been gradually developed from passive response to active control of electromagnetic wave. Different manipulation methods have been explored including external applied electronic field, optical pumping, temperature control, and so on. Various controllable devices based metasurface have been developed.[1–5] Although these reported studies have increased the freedom of metasurface regulation, they have many additional requirements on the composition of materials, structural design or working environment, which hinder the metasurface application in active control electromagnetic wave. In order to reduce the demand for external condition of controllable metasurface, Cui *et al.*[6] proposed the concept of digital encoded metasurface to realize electromagnetic wave regulation by means of digital coding in microwave region.[7–13] Furthermore, in 2016, Cui *et al.*[14] introduced the Fourier convolution theorem in digital signal processing into the coding metasurface. By convolution two different coding sequences, electromagnetic wave regulation with any scattering angle was obtained and further improved the regulation flexibility of the coding metasurface. More recently, the vortex beam carrying orbital angular momentum (OAM) has become a important mean of electromagnetic wave regulation. It can be widely used in modern communication systems.[15–19] At present, most of the orbital angular momentum research is focused on the generation of vortex beams from microwave to optical wave regimes.[20–25] But, there are few literature on terahertz vortex beam generator. Furthermore, metasurface combined with Fourier convolution becomes more meaningful for terahertz vortex beam regulation.

In this paper, we propose a new metasurface based on a combined pattern of outer C-shaped ring and inner rectangular ring. By usign Fourier convolution operation, the proposed metasurface can control vortex terahertz wave splitting, anomalous vortex terahertz wave deflection, and manipulate vortex terahertz wave splitting and deflection simultaneously. The simulation results are consistent with the theoretical predictions. The study shows that the flexible manipulation of terahertz vortex beam has a very high application prospect for improving the capacity of terahertz communication system and the sensitivity of terahertz sensing.

2. Convolution operation metasurface

The matesurface sequence is equivalent to the time signal in digital signal processing, while far-field scattering of the metasurface is similar to the frequency domain in digital signal processing. The product of two signals in the time domain can can be converted to the convolution of two signals in the frequency domain, and the digital convolution theorem can be calculated by

$$f(t)\cdot g(t) \xleftrightarrow{\text{FT}} f(\omega)\cdot g(\omega). \tag{1}$$

The near-field distribution and far-field scattering intensity distribution of metasurface are Fourier transform pairs, therefore, the time signal t and frequency signal ω in Eq. (1) can be replaced by x_λ and $\sin\theta$. Then equation (1) can be further expressed as

$$f(x_\lambda)\cdot g(x_\lambda) \xleftrightarrow{\text{FT}} f(\sin\theta)\cdot g(\sin\theta). \tag{2}$$

In which $x_\lambda = \Gamma/\lambda$ is the electrical length. Fortunately, equation (2) can be simplified as a frequency-shift function when the $g(\omega)$ becomes a Dirac-delta function

$$f(t)\cdot \mathrm{e}^{\mathrm{j}\omega_0 t} \xleftrightarrow{\text{FT}} f(\omega)\cdot\delta(\omega-\omega_0) = f(\omega-\omega_0), \tag{3}$$

†Corresponding author. E-mail: lijsh2008@126.com

© 2022 Chinese Physical Society and IOP Publishing Ltd

where $e^{j\omega_0 t}$ is the time-shift item in time domain, and its frequency spectrum expression is $\delta(\omega)$. Equation (3) reveals the convolution of a spectrum function $f(\omega)$ with an impulse function $\delta(\omega-\omega)$, which will cause the spectrum function $f(\omega)$ to shift by ω in the frequency domain. Similarly, the far-field scattering pattern of the metasurface can be obtained as

$$f(x_\lambda)\cdot e^{j\sin\theta_0 x_\lambda} \xleftrightarrow{\text{FT}} F(\sin\theta)\cdot\delta(\sin\theta-\sin\theta_0) = F(\sin\theta-\sin\theta_0), \tag{4}$$

where the item $e^{j\sin\theta_0 x_\lambda}$ describes the metasurface with unity scattering amplitude and gradient phase distribution. Equation (4) demonstrates the product of an initial coded metasurface sequence and an encoded metasurface sequence with gradual phase distribution causes the metasurface far field scattering pattern to deviate from its initial scattering direction. The sum of two encoding metasurface sequences of $f(x_\lambda)$ and $e^{j\sin\theta_0 x_\lambda}$ generates a new encoding sequence $f(x_\lambda)\cdot e^{j\sin\theta_0 x_\lambda}$. The scattering angle of this new coded sequence can be given by $\theta' = \sin^{-1}(\sin\theta_1+\sin\theta_2)$, where θ_1 and θ_2 are the scattering angles of two initial coding sequences. Likely, two coded metasurface sequences of $f(x_\lambda)$ and $e^{j\sin\theta_0 x_\lambda}$ can also be subtracted. In addition, the new scattering angle θ' and φ' can be obtained for Fourier convolution of two orthogonal gradient-encoded sequences as

$$\theta' = \sin^{-1}\left(\sqrt{\sin^2\theta_1+\sin^2\theta_2}\right), \tag{5}$$

$$\varphi' = \tan^{-1}\left(\frac{\sin^2\theta_2}{\sin^2\theta_1}\right). \tag{6}$$

As mentioned above, the beam scattering can be adjusted in arbitrary direction on Fourier convolution operation metasurfacce. In this article, the coding sequence of generation vortex beam can be added to the gradient coding sequence construct a new coding sequence by Fourier convolution operation, which can flexibly manipulate the vortex terahertz beam in transmission mode.

3. Fourier convolution operation metasurface

Figure 1(a) shows three-dimensional (3D) schematic diagram of the designed Fourier convolution operation metasurface element, which consists of metallic bottom layer, polyimide dielectric middle layer, and metallic pattern layer, respectively. The optimized dimensions of the coding element are as follows: $a=60$ μm, $b=56$ μm, $c=30$ μm, $d=26$ μm, $p=100$ μm. Here, the polyimide has relative permittivity $\varepsilon=11.9$ with thickness of $h=49$ μm. Both the top and bottom gold patterns have a thickness of 200 nm. Figure 1(b) displays the top view of coding element by rotating orientation angle (α) of the metallic pattern. For 2-bit coding metasurface, the rotation angle (α) of the coding element varies from 0° to 180° with step width of 22.5°. Figure 1(c) illustrates schematic diagram of multi-function terahertz metasurface. Figures 2(a) and 2(b) show the reflection amplitude and phase of coding particles of "0", "1", "2", and "3" under circularly polarization incidence. One can clearly see from Fig. 2(a) that the reflection amplitudes of the four coding unit cells labeled with numbers "0" to "3" exceed 0.8 at frequency range of 0.6 THz–0.9 THz. Figure 2(b) illustrates the four coding unit cells fully cover the 180° phase range with a 90° interval by changing rotation angle (α) at 0.5 THz–1.2 THz.

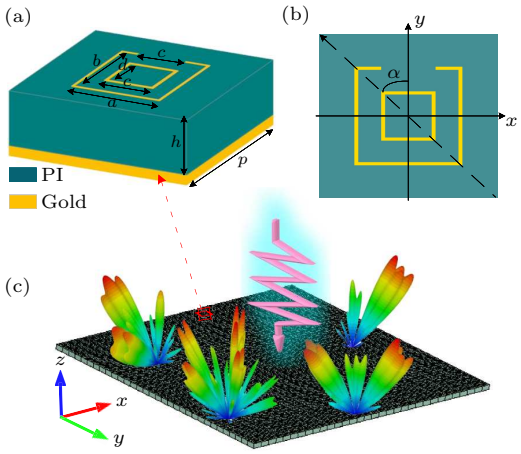


Fig. 1. Coding element structure: (a) 3D plot of coding element; (b) top view of the coding element with rotation angle α; (c) schematic diagram of multi-function terahertz metasurface.

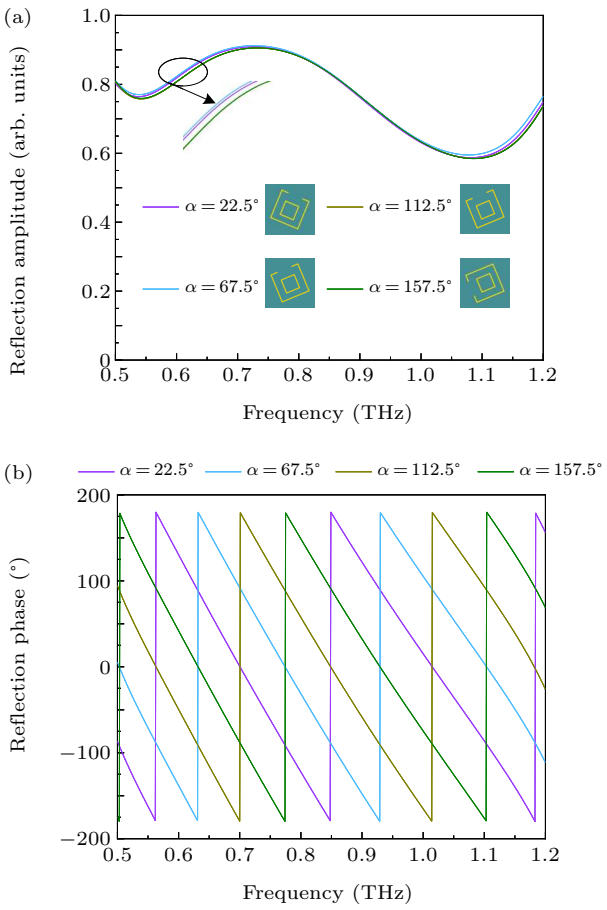


Fig. 2. Reflection amplitude and phase under circularly polarization incidence. (a) reflection amplitude; (b) reflection phase.

3.1. Terahertz vortex beam splitting manipulation

To generate a vortex beam, the metasurface needs to meet the spiral phase distribution of $2n\Delta\varphi = 2\pi l$. Where l is the topological charge that can be taken as any integer, and $2n$ means the 2π area divided into $2\pi/2n$. The phase difference between adjacent areas is fixed at $\Delta\varphi$. According to the generalized Snell's law and the far-field function of metasurface scattering, the relation among the azimuth angle (φ) of reflected terahertz beam, the length and width (Dx and Dy) of the unit cell can be calculated by $\varphi = \pm\arctan(Dx/Dy)$ and $\varphi = \pi \pm \arctan(Dx/Dy)$. The pitch angle ($\theta$), which is related to the corresponding terahertz wavelength (λ) in free space and the length of a gradient periodicity, can be given by $\theta = \arcsin(\lambda/\Gamma)$.

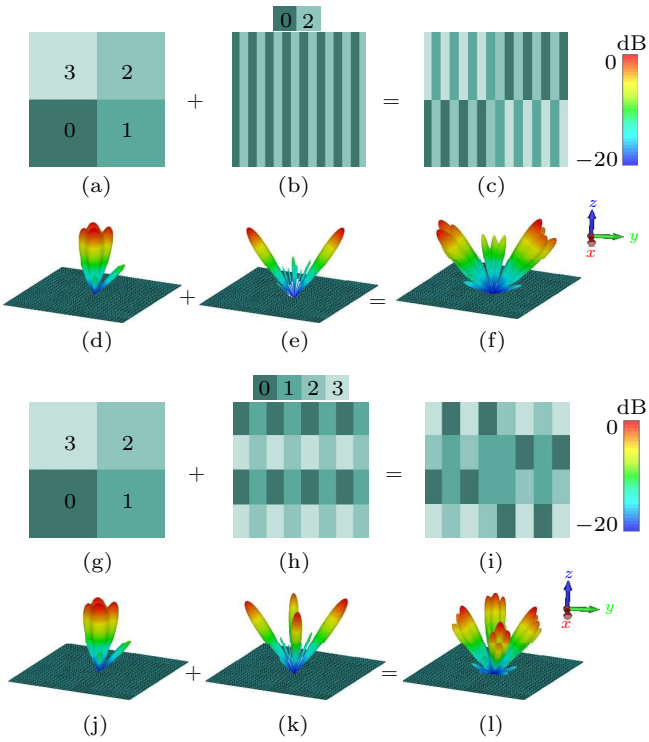


Fig. 3. Vortex terahertz beam spitting control. (a)–(c) Coding patterns operation on 2-bit metasurface. (d)–(f) Related 3D scattering fields of two terahertz vortex beams. (g)–(i) Coding patterns operation on 2-bit metasurface. (j)–(l) Corresponding 3D scattering pattern of four terahertz vortex beams.

Figure 3 shows the reflection vortex terahertz beam splitting by Fourier convolution operation on 2-bit metasurface under the normal incidence terahertz wave. As presented in Figs. 3(a)–3(c), one can noted that the Fourier convolution operation between the vortex terahertz beam coding sequence and the "0000222220000022222⋯" coding sequence arranged along the x axis obtains two vortex terahertz wave coding sequences. The 3D scattering fields of two terahertz vortex beams under right-handed circularly polarized (RCP) (left-handed circularly polarized (LCP)) at frequency of 0.68 THz are vertically incident on the designed metasurface, as clearly exhibited in Figs. 3(d)–3(f). As displayed in Figs. 3(g)–3(i), it can be observed that the Fourier convolution operation between the generated vortex terahertz beam coding sequence and the coding sequence arranged in "00001111⋯/22223333⋯" generates four terahertz vortex wave coding sequences. The corresponding 3D far-field scattering patterns of four terahertz vortex beams at frequency of 0.68 THz are depicted in Figs. 3(j)–3(l). Figures 4(a) and 4(b) describe the two-dimensional (2D) electric field intensity distributions of two and four vortex terahertz beams, respectively. It can be seen from the figure that the incident terahertz wave produces two reflected terahertz vortex beams ($\theta = 33°$, $\varphi = 0°$, $180°$) and four reflected terahertz vortex beams ($\theta = 33°$, $\varphi = 0°$, $90°$, $180°$, $270°$). The corresponding 2D scattering patterns of vortex terahertz beams as shown in Fig. 5. Figure 5(a) gives the 2D scattering pattern of two beams at the azimuth angle of $0°$. Figure 5(b) shows the 2D scattering pattern of four beams at the azimuth angle of $0°$. According to Figs. 3 and 4, one can see that the number and reflection direction of terahertz vortex beams are controlled by the convolution operation coding metasurface.

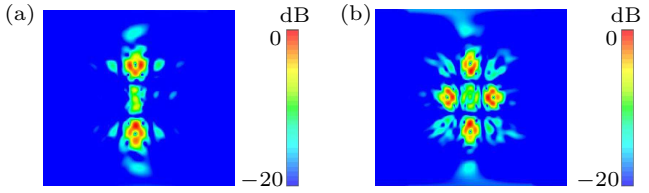


Fig. 4. Electric field intensity distributions of vortex beams: (a) two vortex beams, (b) four vortex beams.

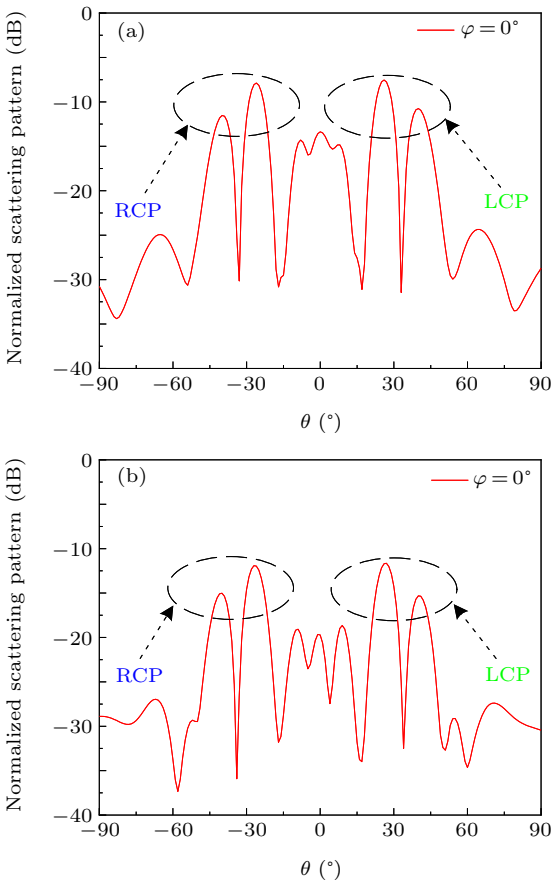


Fig. 5. 2D scattering patterns of vortex terahertz beams: (a) two vortex beams at the azimuth angle of $0°$; (b) four vortex beams at the azimuth angle of $0°$.

3.2. Terahertz vortex beam anomalous deflection manipulation

Figure 6 shows the deflection control of reflected terahertz wave vortex beam on a Fourier convolution operation 2-bit metasurface. As depicted in Figs. 6(a)–6(c), one can find that the coding patterns of generating deflected terahertz vortex beam is obtained by Fourier convolution of "000111222333···" coding sequence arranged along the y axis and the generation of terahertz vortex beam coding sequence. Figures 6(d)–6(f) illustrates the 3D far-field scattering pattern of deflected terahertz vortex beam at frequency of 0.68 THz under the incident RCP (LCP) terahertz wave on the proposed metasurface. Figures 7(a) and 7(b) display the normalized intensity distribution and the phase distribution of coding pattern in Fig. 6(b) respectively. Electric field intensity distributions and 2D scattering pattern of vortex terahertz beams are shown in Fig. 8. Figure 8(a) illustrates the electric field intensity distributions of deflected terahertz vortex beam and figure 8(b) describes the 2D scattering pattern of deflected terahertz vortex beam at the azimuth angle of 0°. From Figs. 7 and 8, one can noted that the terahertz vortex beam deflection can be controlled by the convolution operation of the vortex terahertz beam coding sequence and the gradient coding sequence.

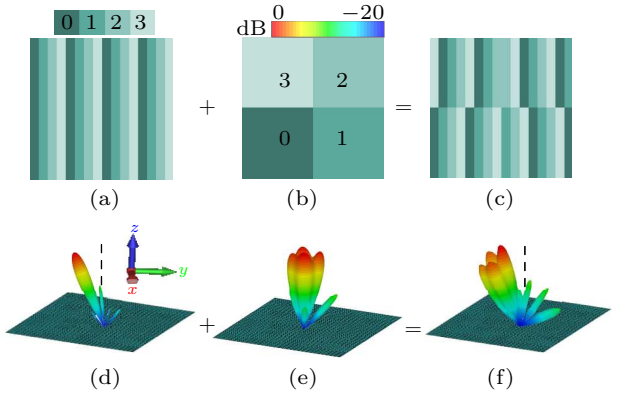


Fig. 6. Vortex terahertz beam anomalous deflection control: (a)–(c) coding patterns operation on a 2-bit metasurface; (d)–(f) 3D scattering fields of deflected vortex terahertz beam.

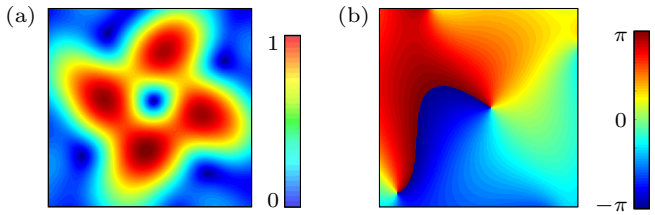


Fig. 7. Near-field and phase distributions of the proposed coding pattern in Fig. 6(b), (a) normalized intensity distribution; (b) phase distribution.

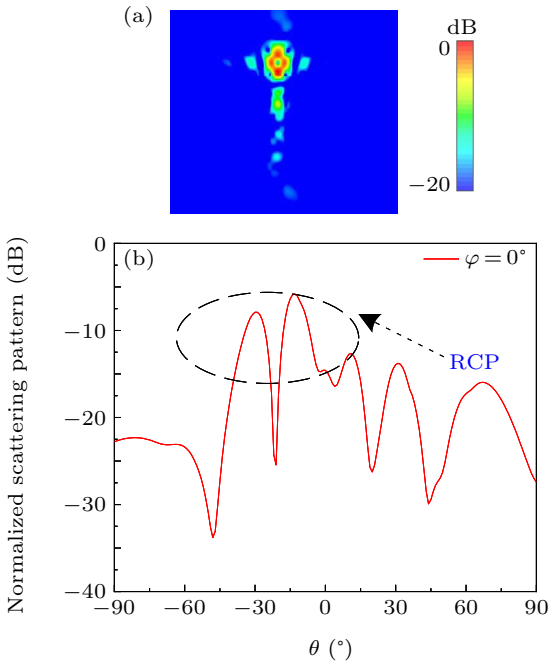


Fig. 8. Electric field intensity distributions and 2D scattering pattern of terahertz vortex beams. (a) Electric field intensity distributions, (b) 2D scattering pattern of the deflected vortex beam at the azimuth angle of 0°.

3.3. Terahertz vortexbeam splitting and deflection manipulation simultaneously

In addition, we can observe clearly from Fig. 9 that the incident terahertz wave generates the reflected terahertz vortex beam splitting and deflection control simultaneously. As shown in Figs. 9(a)–9(d), it can be noted that the coding patterns of generating two deflected vortex beams is obtained by Fourier convolution operation of the coding sequence "00112233···" arranged along the x direction, the coding sequence "000022222000022222···" arranged along the y direction and the coding sequence generated terahertz vortex beam. Under the RCP (LCP) terahertz wave normal incidence, the related 3D far-field scattering patterns of two deflected terahertz vortex beams at frequency of 0.68 THz are exhibited in Figs. 9(i)–9(l). As presented in Figs. 9(e)–9(h), we observe that the coding patterns of generating four deflected vortex beams is obtained by performing Fourier convolution operation of the coding sequence "000011122223333···" along the x direction, the coding sequence "000000222222···/222222000000···" and the coding sequence generated terahertz vortex beam. The corresponding 3D scattering far-fields of four deflected terahertz vortex beams at frequency of 0.8 THz, as displayed in Figs. 9(m)–9(p). When the terahertz wave is perpendicularly incident on the metasurface composed of the coding sequence in Fig. 9(d), the incident terahertz wave generates two reflected terahertz vortex beams with a deflection angle of 33° (see Fig. 9(l)). At this time, the deflection angle of 33° is controlled by the "0000222220000022222···" coding sequence arranged along the y axis. Similarly, when the terahertz wave is perpendicularly incident on the metasurface composed of the coding sequence in Fig. 9(h), four reflected terahertz vortex beams are generated with a deflection angle of 18° (see Fig. 9(p)), which is controlled by the "000011122223333···" coding sequence arranged along the y axis. Figures 10(a) and 10(b)

show the two-dimensional electric field distribution of two and four vortex terahertz wave deflections, respectively. It can be seen clearly from the figure that both two and four terahertz vortex beams deviate from the center point. It can be found from Figs. 9 and 10 that the convolution operation between the vortex terahertz beam coding sequence and different coding sequences can generate multiple terahertz wave vortex beams with different deflective scattering angles.

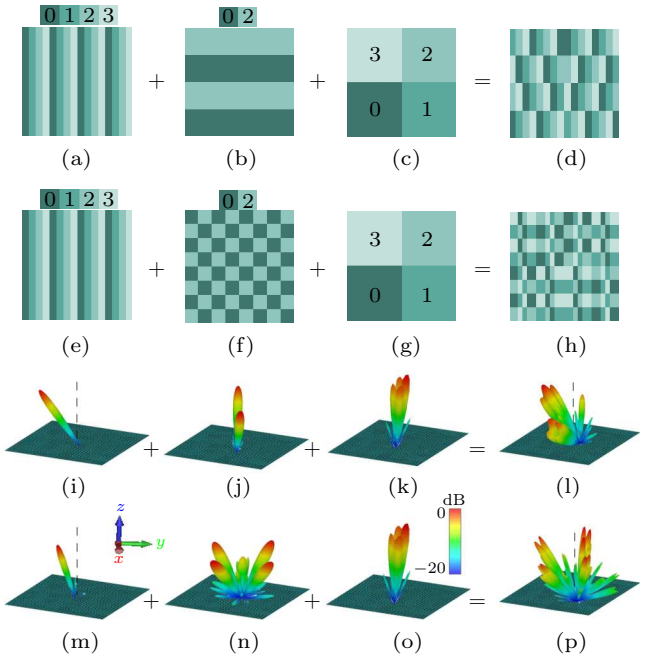


Fig. 9. Vortex terahertz beam splitting and deflection control. (a)–(h) Coding patterns operation on a 2-bit metasurface. (i)–(l) Related 3D scattering fields of two deflected vortex terahertz beams. (m)–(p) Corresponding 3D scattering fields of four deflected vortex terahertz beams.

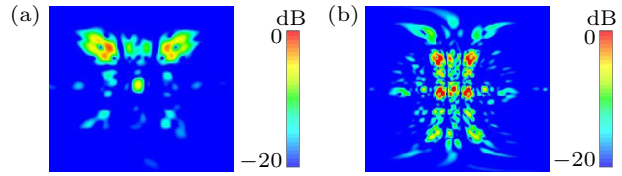


Fig. 10. Electric field intensity distributions of vortex terahertz beams. Two beams (a), four beams (b) deflected vortex terahertz wave beams.

4. Conclusion

In summary, we proposed a novel Fourier convolution operation metasurface, which is made of bottom metal layer, intermediate dielectric layer, and top metal pattern with a combined pattern of outer C-shaped ring and inner rectangular ring. A coding sequence generated by Fourier convolution, the presented metasurface can realize multi-function manipulation for the incident terahertz wave, such as multi terahertz beams, terahertz vortex beam with arbitrary scattering angle, and multi terahertz vortex beam with a certain deflection angle. The study provides a new idea for flexible control of terahertz vortex beam, and also offers an effective method for terahertz wave manipulation.

Acknowledgments

Project supported by the National Natural Science Foundation of China (Grant Nos. 61871355 and 61831012), the Talent Project of Zhejiang Provincial Department of Science and Technology (Grant No. 2018R52043), and the Research Funds for Universities of Zhejiang Province, China (Grant Nos. 2020YW20 and 2021YW86).

References

[1] Chen M, Sun W, Cai J J, Chang L Z and Xiao X F 2017 *Opt. Commun.* **382** 144
[2] Liu Z and Bai B 2017 *Opt. Express* **25** 8584
[3] Zhao J C, Cheng Y Z and Cheng Z Z 2018 *IEEE Photon. J.* **10** 4600210
[4] Ding F, Zhong S M and Bozhevolnyi S I 2018 *Adv. Opt. Mater.* **6** 1701204
[5] Wang T, He J W, Guo J Y, Wang X, Feng S F, Kuhl F, Becker M, Polity A, Klar P J and Zhang Y 2019 *Opt. Express* **27** 20347
[6] Cui T J, Qi M Q, Wan X, Zhao J and Cheng Q 2014 *Light: Sci. Appl.* **3** e218
[7] Feng M C, Li Y F, Zheng Q Q, Zhang J Q, Han Y J, Wang J F, Chen H Y, Sai S, Ma and Qu S B 2018 *J. Phys. D: Appl. Phys.* **51** 375103
[8] Shao L, Premaraten M and Zhu W R 2019 *IEEE Access* **7** 45716
[9] Saifullah Y, Waqas A B, Yang G M and Xu F 2020 *Opt. Express* **28** 1139
[10] Yang J J, Cheng Y Z, Qi D and Gong R Z 2018 *Appl. Sci.* **8** 1231
[11] Cui T J, Liu S and Zhang L 2017 *J. Mater. Chem. C* **5** 3644
[12] Yang S, Guan C S, Ding X M, Zhang K, Burokur S N and Wu Q 2021 *Photonics* **8** 174
[13] Han X M, Xu H J, Chang Y P, Lin M, Zhang W Y, Wu X and Wei X L 2020 *IEEE Access* **8** 162313
[14] Liu S, Cui T J, Zhang L, Xu Q, Wang Q, Wan X, Gu J Q, Tang W X, Qi M Q, Han J G, Zhang W L, Zhou X Y and Cheng Q 2016 *Adv. Sci.* **3** 1600156
[15] Zhao Y F, Yao Y, Xu K, Yang Y and Tian J J 2020 *Opt. Commun.* **475** 126165
[16] Xiong X W, Zheng S L, Zhu Z L, Wang Z X, Chen Y Q, Yu X B and Zhang X M 2020 *IEEE Commun. Lett.* **24** 2628
[17] Zhu C J, Song M Z and Dang X Y 2020 *Radioengineering* **29** 563
[18] Jiang X, Ta D and Wang W Q 2020 *Phys. Rev. Appl.* **14** 034014
[19] Iqbal S, Akram M R, Furqan M, Madni H A, Khan M I and Shu G X 2020 *IEEE Access* **8** 197982
[20] Zhang C, Xu P F and Jiang X F 2020 *AIP Adv.* **10** 105230
[21] Shi Y, Wu Q W and Ming J 2021 *IEEE Access* **9** 63122
[22] Feng H, Ye L F, Zhang Y Y, Li W W, Chen H Y and Liu Q H 2020 *Appl. Phys. Lett.* **117** 241601
[23] Liu B, He Y J, Wong S W and Li Y 2020 *Adv. Opt. Mater.* **9** 2001689
[24] Ge Y F, Wu Y P, Zang X F, Yuan Y H and Chen L 2020 *Acta Phys. Sin.* **69** 184203 (in Chinese)
[25] Chen L, Liao D G, Guo X G, Zhao J Y, Zhu Y M and Zhuang S L 2019 *Front. Inform. Technol. Elect. Eng.* **20** 591